Brinkman-Forchheimer Slip Flow of Hybrid Nanofluid through a Flat Plate with Thermal Radiation: A Cattaneo-Christov Heat Flux Model

M. Sreenivasulu*[1a], R. Bhuvana Vijaya[1b]

[1]Department of Mathematics, JNTUA College of Engineering, Ananthapuramu – 515 002, India. seenuu.atp@gmail.com[1a], bhuvanarachamalla.maths@jntua.ac.in[1b]

Article Info
Page Number: 1077-1089
Publication Issue:
Vol. 72 No. 1 (2023)

Article History
Article Received: 15 October 2022
Revised: 24 November 2022
Accepted: 18 December 2022

Abstract: The purpose of this work is to examine the influence of the velocity slip parameter and viscous dissipation on the features of the flow of a radiative hybrid nanofluid (Ethylene Glycol + Graphene + Copper) past a flat plate. Additionally, Cattaneo-Christov model is merged in the energy equation. The equations required to represent the problem have been turned into a system, and this system has been solved using the bvp4c solver. The heat transmission rate and friction factor against the pertinent parameters are explained using bar graphs. It is observed that, at $0 \le Mn \le 3$, (Magnetic field parameter), friction factor declines at a proportion of 0.07462 and the rate of increment in the friction factor is 0.385017 when volume fraction of graphene nanoparticles (ϕ_g) is in the range $0 \le \phi_g \le 0.25$. Nusselt number is found to decrease by 0.85144 when Eckert number (Eck) is adjusted to $0.1 \le Eck \le 0.6$, while the same increases by 0.350461 when $0 \le \Lambda \le 0.25$ (thermal relaxation parameter) is used. Temperature has been seen to rise with increases in the thermal radiation parameter. In addition, it has been shown that a diminution in the velocity profile takes place whenever the porosity parameter is increased.

Keywords: Thermal radiation, Hybrid nanofluid, Flat plate, Cattaneo-Christov heat flux, Viscous dissipation, Velocity slip.

Nomenclature

$\kappa\left(=\kappa_0 x\right)$	Permeability of porous medium	η	Similarity variable
σ	Electrical conductivity	σ^*	Stefan-Boltzmann constant
$\Pr$	Prandtl number	Λ	Thermal relaxation parameter
k^*	Mean absorption coefficient	Mn	Magnetic field Parameter
υ	Kinematic viscosity	u, v	Components of velocity in two (x, y) directions
k	Thermal conductivity		
ϕ_g	Volume fraction of Graphene	$C_1\left(=\frac{C_0}{\sqrt{x}}\right)$	Coefficient of porous inertia (second order)
ϕ_c	Volume fraction of Copper		

g Acceleration due to gravity	L Slip length
Eck Eckert number	$\lambda_1 \left(= \lambda_0 x\right)$ Thermal relaxation time of heat flux
S Velocity slip parameter	Rd Thermal radiation parameter
δ Porosity parameter	
Γ Porous media (second order) resistance parameter	
λ Mixed convection parameter	
C_p Specific heat capacity	

1 Background Information

Nanofluids are a novel and intriguing class of heat transmission fluids that can be used in place of more conventional options. As a result of their diminutive size, they may greatly reduce erosion and corrosion. Fuel cells, heat exchangers, and pharmaceutical process are just a few of the many uses for them. When more than one nanoparticle is present in a nanofluid, it is called a hybrid nanofluid, which differs from mono nanofluid. Thus, when compared to mono fluids, the heat transmission properties of hybrid fluids are superior. These are finding uses in a wide variety of fields, from solar energy to air conditioning. Huang et al. [1] conducted an experiment to investigate the characteristics of heat transmission by analyzing an HNF flow (water, alumina, and MWCNTs) that took place inside of a heat exchanger. According to the findings of Rahman et al. [2], the friction factor is up whenever there is an increase in the number of hybrid nanoparticles. According to research conducted by Rahman et al. [2], the friction coefficient rises with each additional hybrid nanoparticle. Theoretical work by Iqbal et al. [3] examined the passage of HNF through a rotating erect channel, using radiation and Hall current. An increase in temperature can be explained by an increase in the rate of thermal radiation. Amala and Mahanthesh [4] discussed an HNF flow that included a heat sink by taking into consideration a revolving plate. It has been discovered that increasing the nanoparticle volume percentage makes the temperature field stronger. According to Alharbi et al. [5], the hybrid nanofluid generates heat at a faster pace than the nanofluid itself. To examine the radiative flow of a HNF caused by a spinning disc, Acharya et al. [6] enacted a combination of shooting and RK4 procedures. Nadeem et al. [7] examined a HNF (Water + Cu + Al_2O_3) flow by a curved extending surface with suction/injection. Different behaviors were seen depending on the injection/suction when volume % of Al_2O_3 is applied on temperature profile. Waini et al. [8] scrutinized the stagnation point flow of the same HNF by the use of a cylinder and offered two different solutions. It has been observed that as the Reynolds' number surges, the temperature of the fluid drops. After that, a number of scholars [9-14] investigated different hybrid nanofluid flows by taking into consideration a variety of geometries.

The CCHF model (Cattaneo - Christov heat flux) does a good job of representing heat transport processes because it is based on a modified version of the model of heat conduction introduced by Fourier and subsequently enhanced by Cattaneo. Oldroyd's derivative and the time required for thermal relaxation are taken into account in this model. UCM fluid flow was studied by Shah et al. [15], who analyzed the impression of Ohmic heating using an expanding sheet and the CCHF model. The conclusion drawn is that a higher Deborah number causes a fluid's temperature to rise. With the same concept and geometry in mind, Khan and Khan [16] investigated the 3D flow of Burgers fluid. Temperatures were more evenly distributed according to Fourier's law than the CCHF model predicted. In their study of nanofluid flow, Xu and Chen [17] observed that the heat transmission rate is bigger for the minor shape feature of the nanoparticle. With the help of HAM, Vasu and Ray [18] discussed the Carreau fluid flow over an erect plate using the CCHF model. It has been demonstrated that shear thickening fluids have a lower surface shear stress than shear thinning fluids. Ali et al. [19] inspected a viscous fluid flow by a revolving disk with heat sink/source in the slip regime. Using the CCHF model, Abu-Hamdeh et al. [20] carried on a computational study of nanofluid flow through a porous extended surface. Research shows that when the Reynolds number increases, so does the entropy. In later studies [21–24], a variety of authors used the CCHF model to investigate diverse fluid flows.

In view of the preceding research, nobody has up until now tried to explain the significance of non-Fourier heat flux and viscous dissipation effects, for the radiative hybrid nanofluid (Ethylene glycol + Graphene + Copper) flow. Engineering parameters of concern including friction factor are explained using bar graphs. The concept of Cattaneo-Christov (C-C) Heat Flux (H - F) has been added into the energy equation with the purpose of discussing the characteristics of heat transmission.

2 Research Methodology

In this study, a laminar, steady and dissipative hybrid nanofluid (Ethylene Glycol + Graphene + Copper) flow through a flat plate with thermal radiation and velocity slip parameter is considered. Thermophysical characteristics of Ethylene Glycol (base fluid), Graphene and Copper (nanoparticles) are shown in Table 1. Following are the assumptions for the current study:

(i) The $x-$ axis is supposed to be parallel to the plate and the $y-$ axis is perpendicular to it.

(ii) Over the surface of the plate, the fluid is moving at a constant speed U_∞ (see Fig. 1).

(iii) There is a magnetic field applied perpendicular to the direction of flow, with a strength of $B = \frac{B_0}{\sqrt{x}}$.

(iv) Moreover, the momentum equation incorporates the Darcy-Brinkmann model

and the energy equation includes the Cattaneo-Christov model of heat flux.

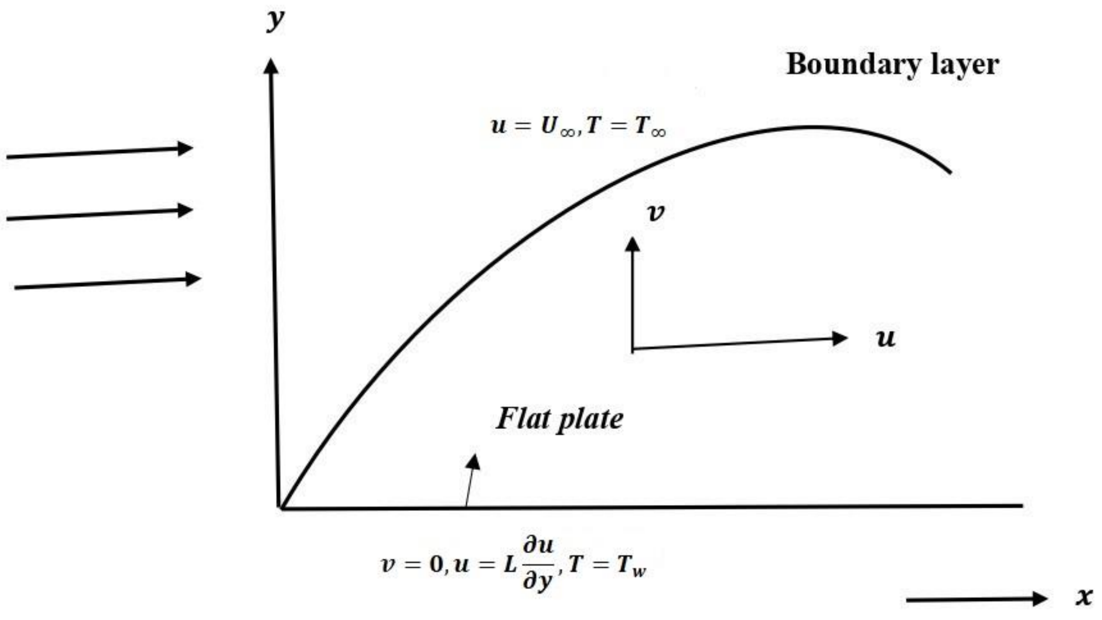

Fig. 1 Schematic diagram

These assumptions lead to the following conditions and equations: (Rao et al. [21], Makinde [25] and Shehzad et al. [26])

$$\frac{\partial}{\partial x}(u)+\frac{\partial}{\partial y}(v)=0 \tag{1}$$

$$u\frac{\partial}{\partial x}(u)+v\frac{\partial}{\partial y}(u)=\upsilon_{hnf}\frac{\partial^2}{\partial y^2}(u)-\frac{\upsilon_{hnf}}{\kappa}u+g\left(T-T_\infty\right)\beta_T-\frac{C_1}{\rho_{hnf}}\frac{1}{\sqrt{\kappa}}u^2-B^2\frac{\sigma_{hnf}}{\rho_{hnf}}u \tag{2}$$

$$\begin{aligned}
&u\frac{\partial}{\partial x}(T)+v\frac{\partial}{\partial y}(T)=\left(\frac{1}{\rho C_p}\right)_{hnf}k_{hnf}\frac{\partial^2}{\partial y^2}(T)+\left(\frac{1}{\rho C_p}\right)_{hnf}\left(\frac{\partial}{\partial y}(u)\right)^2\mu_{hnf}\\
&-\lambda_1\left[\begin{array}{l} u^2\dfrac{\partial^2}{\partial x^2}(T)+2uv\dfrac{\partial}{\partial x}\left(\dfrac{\partial}{\partial y}(T)\right)+v^2\dfrac{\partial^2}{\partial y^2}(T)+\dfrac{\partial}{\partial y}(T)\left(u\dfrac{\partial}{\partial x}(v)+v\dfrac{\partial}{\partial y}(v)\right)\\ +\dfrac{\partial T}{\partial x}\left(u\dfrac{\partial}{\partial x}(u)+v\dfrac{\partial}{\partial y}(u)\right)\end{array}\right]\\
&+\left(\frac{1}{\rho C_p}\right)_{hnf}\frac{4}{3}\frac{4\sigma^* T_\infty^3}{k^*}\frac{\partial^2}{\partial y^2}(T)
\end{aligned} \tag{3}$$

$$\left.\begin{array}{l} u(x,y)\big|_{y=0}=L\dfrac{\partial u}{\partial y}(x,y)\Big|_{y=0},v(x,y)\big|_{y=0}=0,T(x,y)\big|_{y=0}=T_w,\\ u(x,y)\big|_{y=\infty}=U_\infty,T(x,y)\big|_{y=\infty}=T_\infty. \end{array}\right\} \tag{4}$$

2.1 Hybrid nanofluid (HNF) thermophysical characteristics

$$\left.\begin{array}{l}
k_{hnf}=k_{nf}\times\dfrac{k_c+2k_{nf}-2k_{nf}\phi_c+2k_c\phi_c}{k_c+2k_{nf}+k_{nf}\phi_c-k_c\phi_c},\\
\rho_{hnf}=\left[\left(1-\phi_g\right)\rho_f+\phi_g\rho_g\right]\left(1-\phi_c\right)+\rho_c\phi_c,\\
\left(\rho C_p\right)_{hnf}=\left[\left(1-\phi_g\right)\left(\rho C_p\right)_f+\phi_g\left(\rho C_p\right)_g\right]\left(1-\phi_c\right)+\left(\rho C_p\right)_c\phi_c,\\
\sigma_{nf}=\sigma_f\times\dfrac{\sigma_g+2\sigma_f-2\sigma_f\phi_g+2\sigma_{s_1}\phi_g}{\sigma_g+2\sigma_f+\sigma_f\phi_g-\sigma_g\phi_g},\\
k_{nf}=k_f\times\dfrac{k_g+2k_f-2k_f\phi_g+2k_g\phi_g}{k_g+2k_f+k_f\phi_g-k_g\phi_g},\mu_{hnf}=\dfrac{\mu_f}{\left(1-\phi_g\right)^{2.5}\left(1-\phi_c\right)^{2.5}},\\
\sigma_{hnf}=\sigma_{nf}\times\dfrac{\sigma_c+2\sigma_{nf}-2\sigma_{nf}\phi_c+2\sigma_c\phi_c}{\sigma_c+2\sigma_{nf}+\sigma_{nf}\phi_c-\sigma_c\phi_c}.
\end{array}\right\}$$

Table 1 Estimations of distinct properties of ethylene glycol, graphene and copper (Alhowaity et al. [27])

S. No.		Ethylene Glycol (f)	Graphene (s_1)	Copper (s_2)
1	$\rho\left(kgm^{-3}\right)$	1114	2250	8933
2	$k\left(W\left(m\,K\right)^{-1}\right)$	0.252	2500	401
3	$\sigma\left(Sm^{-1}\right)$	5.5 x 10^{-6}	1.0 x 10^{7}	5.96 x 10^{7}
4	$C_p\left(J\left(kg\,K\right)^{-1}\right)$	2415	2100	385

Makinde [25] recommended the succeeding similarity variables to alter controlling equations:

$$\left.\begin{array}{l}
u=U_\infty f'(\eta)=U_\infty\dfrac{d}{d\eta}(f),v=\sqrt{\dfrac{\upsilon U_\infty}{4x}}\left[\eta f'(\eta)-f(\eta)\right],\\
\theta(\eta)=\dfrac{T-T_\infty}{T_w-T_\infty},\eta=y\sqrt{\dfrac{U_\infty}{\upsilon x}}.
\end{array}\right\}$$

(5)

Then (5) makes (1) to fulfil and redraft (2 –4) as:

$$\frac{2}{Q_1Q_2}f'''+2\lambda\theta+ff''-\frac{2Q_3}{Q_1}Mnf'-\frac{2}{Q_1Q_2}\delta f'-\frac{2}{Q_1}\Gamma f'^2=0$$

(6)

$$\left(\frac{Q_4}{Q_5}\frac{2}{\Pr}+\frac{Rd}{Q_5}\frac{2}{\Pr}-\frac{\Lambda}{2}f^2\right)\theta''-\frac{3\Lambda}{2}ff'\theta'+f\theta'+\frac{2}{Q_5Q_2}Eckf''^2=0 \tag{7}$$

$$\left.\begin{aligned}&f(\eta)\big|_{\eta=0}=0,\ f'(\eta)=\frac{d}{d\eta}(f)\bigg|_{\eta=0}=Sf''(\eta)=S\frac{d^2}{d\eta^2}(f)\bigg|_{\eta=0},\\&\theta(\eta)\big|_{\eta=0}=1,\ f'(\eta)=\frac{d}{d\eta}(f)\bigg|_{\eta=\infty}=1,\theta(\eta)\big|_{\eta=\infty}=0.\end{aligned}\right\} \tag{8}$$

where

$$\left.\begin{aligned}&Rd=\frac{4}{3}\frac{4\sigma^*T_\infty^3}{k^*k},\lambda=\frac{Gr_x}{\mathrm{Re}_x^2},Gr_x=\frac{g\beta_T\left(T_w-T_\infty\right)x^3}{\upsilon^2},\mathrm{Re}_x=\frac{U_\infty x}{\upsilon},\delta=\frac{\upsilon}{\kappa_0U_\infty},\\&Mn=\frac{\sigma B_0^2}{\rho U_\infty},\Gamma=\frac{C_0}{\rho\sqrt{\kappa_0}},\Lambda=\lambda_0U_\infty,\Pr=\frac{\mu C_p}{k},Eck=\frac{U_\infty^2}{C_p\left(T_w-T_\infty\right)},S=L_0\sqrt{\frac{U_\infty}{\upsilon}}.\end{aligned}\right\}$$

and

$$\left.\begin{aligned}&Q_2=\left(1-\phi_g\right)^{2.5}\left(1-\phi_c\right)^{2.5},Q_5=\left(1-\phi_c\right)\left[\left(1-\phi_g\right)+\phi_g\frac{\left(\rho C_p\right)_g}{\left(\rho C_p\right)_f}\right]+\phi_c\frac{\left(\rho C_p\right)_c}{\left(\rho C_p\right)_f},\\&Q_{31}=\frac{\sigma_g+2\sigma_f-2\phi_g\left(\sigma_f-\sigma_g\right)}{\sigma_g+2\sigma_f+\phi_g\left(\sigma_f-\sigma_g\right)},Q_1=\left(1-\phi_c\right)\left[\left(1-\phi_g\right)+\phi_g\frac{\rho_g}{\rho_f}\right]+\phi_c\frac{\rho_c}{\rho_f},\\&Q_3=\frac{\sigma_c+2Q_{31}\sigma_f-2\phi_c\left(Q_{31}\sigma_f-\sigma_c\right)}{\sigma_c+2Q_{31}\sigma_f+\phi_c\left(Q_{31}\sigma_f-\sigma_c\right)}Q_{31},Q_4=\frac{k_c+2Q_{41}k_f-2\phi_c\left(Q_{41}k_f-k_c\right)}{k_c+2Q_{41}k_f+\phi_c\left(Q_{41}k_f-k_c\right)}Q_{41},\\&Q_{41}=\frac{k_g+2k_f-2\phi_g\left(k_f-k_g\right)}{k_g+2k_f+\phi_g\left(k_f-k_g\right)}.\end{aligned}\right\}$$

Coefficient of skin friction (Cf_x) is defined as:

$$Cf_x=\frac{\tau_w}{\rho U_\infty{}^2}\bigg|_{y=0}, \tag{9}$$

where $\tau_w=\mu_{hnf}\left(\frac{\partial u}{\partial y}\right)$.

Rewriting the expression in (9) with (5) yields

$$\sqrt{\mathrm{Re}_x}Cf_x = \frac{1}{Q_2} f''(0).$$

Nusselt number can be determined using the following formula:

$$Nu_x = -\frac{xq_w}{k_f\left(T_w - T_\infty\right)}\bigg|_{y=0}. \tag{10}$$

The formula in (10) is reworked with the help of (5) as:

$$\sqrt{\frac{1}{\mathrm{Re}_x}}Nu_x = -Q_4\theta'(0).$$

3 Results and Discussion

In order to solve equations (6 - 7) with the conditions (8), the built-in function bvp4c of MATLAB is employed.

3.1 Profiles of Engineering Parameters of Concern

According to Figs. 2 - 3, it has been noted that Mn diminishes Cf_x, while ϕ_g increases it. It is observed that, at $0 \le Mn \le 3$, the skin friction coefficient declines at a rate of 0.07462 and the rate of increment in the friction factor is 0.385017 when ϕ_g is in the range $0 \le \phi_g \le 0.25$. It is noticed from Figs. 4 – 5 that Eck and Λ have different behaviours on heat transmission rate. When Eck is equal to $0.1 \le Eck \le 0.6$, the heat transfer rate (Nusselt number) is found to decrease by 0.85144 and at $0 \le \Lambda \le 0.25$, the heat transmission rate upsurges at a rate of 0.350461.

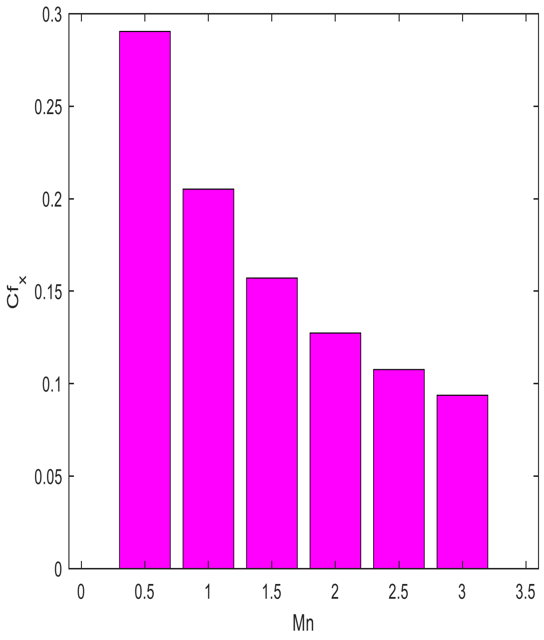

Fig. 2 Profile of skin friction coefficient with the impact of Mn

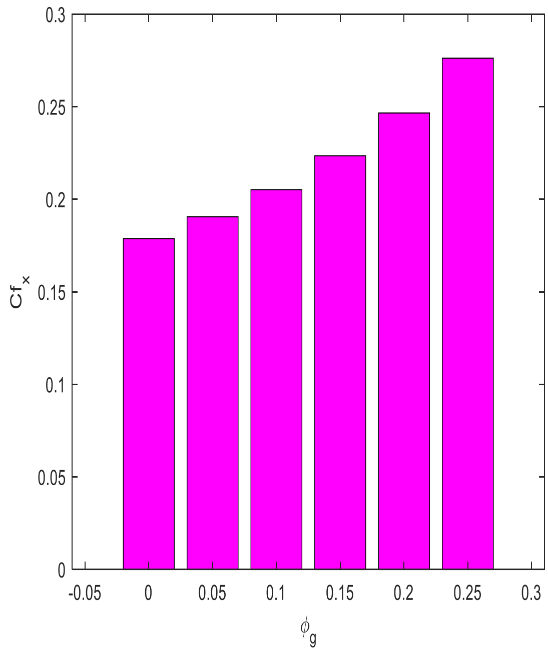

Fig. 3 Profile of skin friction coefficient with the impact of ϕ_g

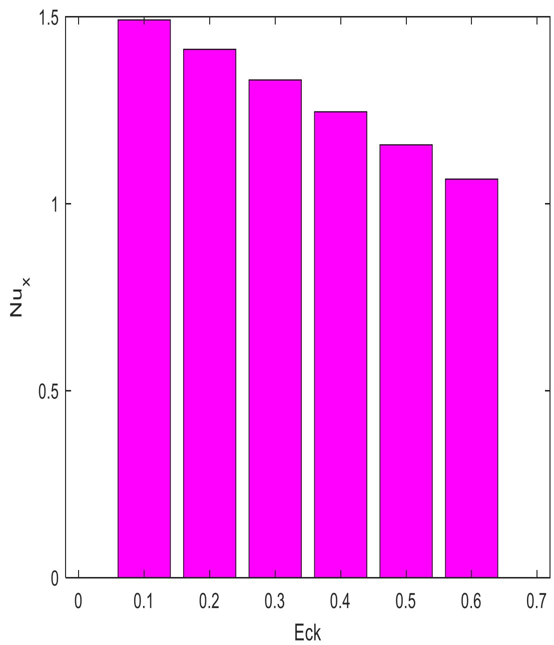

Fig. 4 Profile of Nusselt number with the impact of Eck

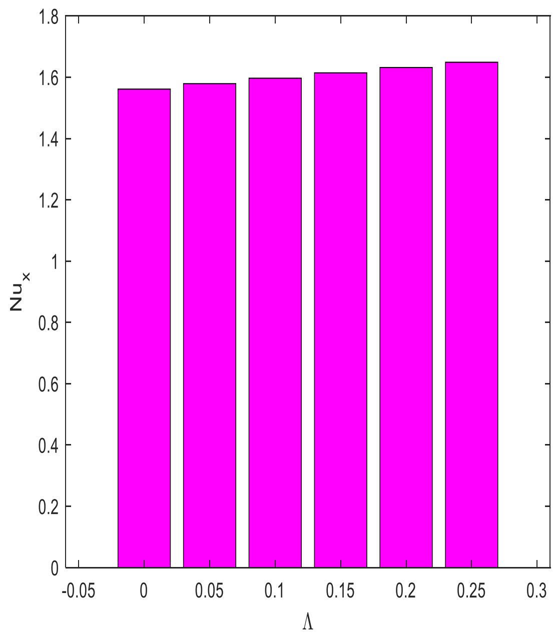

Fig. 5 Profile of Nusselt number with the impact of Λ

3.2 Temperature and Velocity Profiles

As a result of the thermal radiation parameter, heat is transferred to the fluid. There will be a greater transfer of heat energy from the source to the fluid if this value is made larger. Therefore, as seen in Fig. 6, the temperature rises as the fluid particles absorb heat energy. In When Eck grows higher, more of the kinetic energy is transformed into thermal energy by viscous forces. The fluid's temperature therefore increases (see Fig. 7). Temperature reduction in the fluid is seen when the thermal relaxation parameter increases (see Fig. 8). It has been found, as shown in Fig. 9, that when the magnetic field parameter upsurges, the velocity declines. Magnetic flow lines travelled normally through the fluid when an external magnetic field was applied around it. Particles' movement from one layer to another is impeded as a result of the Lorentz force that is created. Due to this, the fluid's molecules travel very slowly. The fluid's velocity slows as a result. In Fig. 10, we can see that when the porosity parameter rises, the fluid's velocity declines. According to the Fig. 11, it has been established that an increase in Γ results in a decrease in velocity.

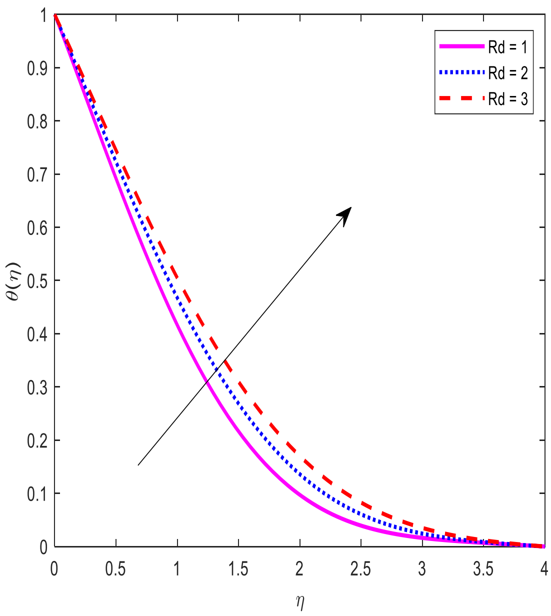

Fig. 6 Profile of $\theta(\eta)$ with the impact of Rd

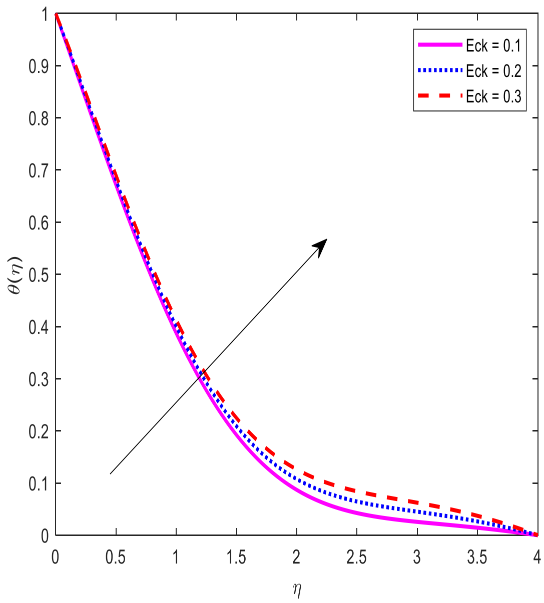

Fig. 7 Profile of $\theta(\eta)$ with the impact of Eck

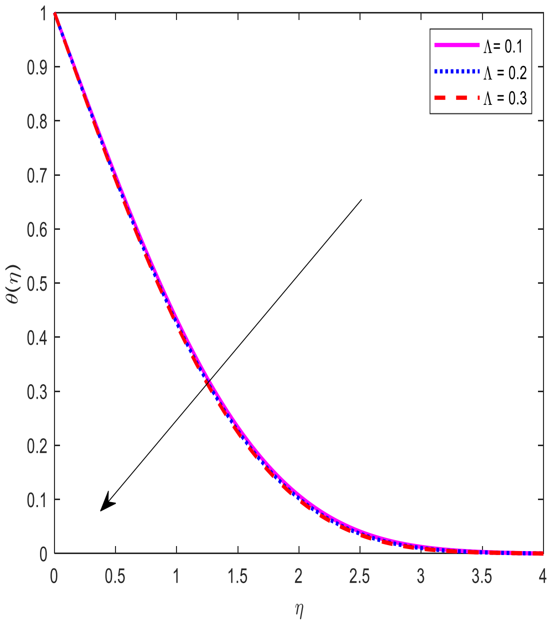

Fig. 8 Profile of $\theta(\eta)$ with the impact of Λ

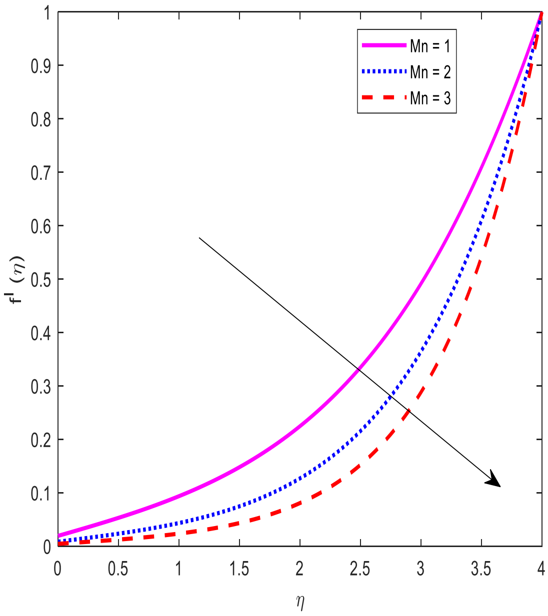

Fig. 9 Profile of $f'(\eta)$ with the impact of Mn

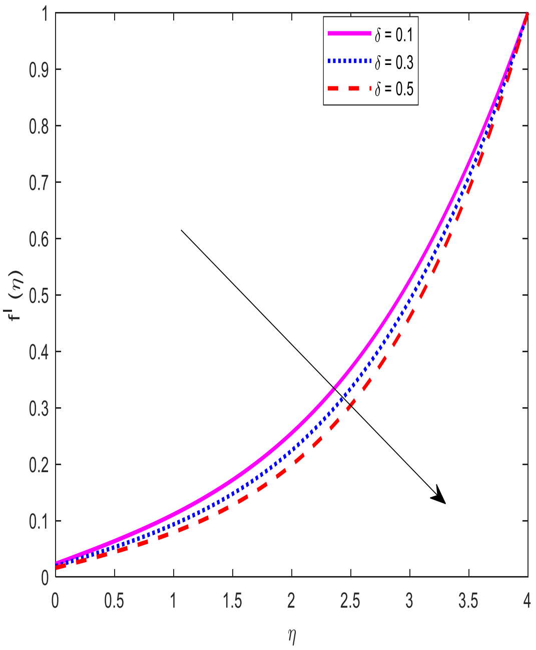

Fig. 10 Profile of $f'(\eta)$ with the impact of δ

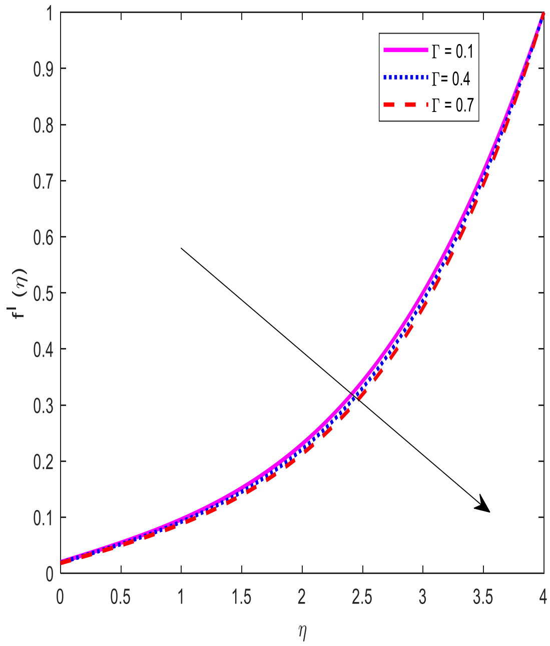

Fig. 11 Profile of $f'(\eta)$ with the impact of Γ

4 Conclusions

The purpose of this work is to examine the influence of the velocity slip parameter and viscous dissipation on the features of the flow of a radiative hybrid nanofluid (Ethylene Glycol +

Graphene + Copper) past a flat plate. Additionally, Cattaneo-Christov model is merged in the energy equation. Moreover, the momentum equation incorporates the Darcy-Brinkmann-Forchheimer model. The study's findings are briefly summarised below.

- It is observed that, at $0 \le Mn \le 3$, friction factor declines at a proportion of 0.07462 and the rate of increment in the friction factor is 0.385017 when ϕ_g is in the range $0 \le \phi_g \le 0.25$.
- Nusselt number is found to decrease by 0.85144 when Eck is adjusted to $0.1 \le Eck \le 0.6$, while the same increases by 0.350461 when $0 \le \Lambda \le 0.25$ is used.
- Temperature has been seen to rise with increases in the thermal radiation parameter.
- It has been shown that a drop in the fluid's velocity takes place whenever the porosity parameter is increased.

References

1. Huang D, Wu Z, Sunden B. Effects of hybrid nanofluid mixture in plate heat exchangers. Experimental Thermal and Fluid Science. 2016;72:190-196.
2. Rahman MR, Leong KY, Idris AC, Saad MR, Anwar M. Numerical analysis of the forced convective heat transfer on Al2O3–Cu/water hybrid nanofluid. Heat and Mass Transfer. 2017;53(5):1835-1842.
3. Iqbal Z, Akbar NS, Azhar E, Maraj EN. Performance of hybrid nanofluid (Cu-CuO/water) on MHD rotating transport in oscillating vertical channel inspired by Hall current and thermal radiation. Alexandria engineering journal. 2018;57(3):1943-1954.
4. Amala S, Mahanthesh B. Hybrid nanofluid flow over a vertical rotating plate in the presence of hall current, nonlinear convection and heat absorption. Journal of Nanofluids. 2018;7(6):1138-1148.
5. Dhabliya, D., & Dhabliya, R. (2019). Key characteristics and components of cloud computing. International Journal of Control and Automation, 12(6 Special Issue), 12-18. Retrieved from www.scopus.com
6. Dhabliya, D., & Parvez, A. (2019). Protocol and its benefits for secure shell. International Journal of Control and Automation, 12(6 Special Issue), 19-23. Retrieved from www.scopus.com
7. Dhabliya, D., & Sharma, R. (2019). Cloud computing based mobile devices for distributed computing. International Journal of Control and Automation, 12(6 Special Issue), 1-4. doi:10.33832/ijca.2019.12.6.01
8. Alharbi SO, Nawaz M, Nazir U. Thermal analysis for hybrid nanofluid past a cylinder exposed to magnetic field. AIP Advances. 2019;9(11):115022.
9. Acharya N, Bag R, Kundu PK. Influence of Hall current on radiative nanofluid flow over a spinning disk: a hybrid approach. Physica E: Low-dimensional Systems and Nanostructures. 2019;111:103-112.
10. Nadeem S, Abbas N, Malik MY. Inspection of hybrid based nanofluid flow over a curved surface. Computer Methods and Programs in Biomedicine. 2020;189:105193.
11. Waini I, Ishak A, Pop I. Hybrid nanofluid flow towards a stagnation point on a stretching/shrinking cylinder. Scientific Reports. 2020;10(1):1-2.

12. Venkateswarlu A, Murshid N, Mulki H, Abu-samha M, Suneetha S, Babu MJ, Raju CS, Homod RZ, Al-Kouz W. A Significant Role of Activation Energy and Fourier Flux on the Quadratically Radiated Sphere in Low and High Conductivity of Hybrid Nanoparticles. Symmetry. 2022;14(11):2335.
13. Arshad M, Hassan A. A numerical study on the hybrid nanofluid flow between a permeable rotating system. The European Physical Journal Plus. 2022;137(10):1126.
14. Ramakrishna SB, Avula SR, Sadananda MU, Macherla JB, Chakravarthula SR. Significance of non-Fourier flux on a chemically reactive ternary hybrid nanofluid flow (water+ Al2O3+ ZnO+ Fe3O4) by a quadratically radiated tended elongating surface. ZAMM-Journal of Applied Mathematics and Mechanics/Zeitschrift für Angewandte Mathematik und Mechanik. 2022:e202200103.
15. Krishna MV, Chamkha AJ. Hall and ion slip impacts on Unsteady MHD Convective flow of Ag-TiO2/WEG hybrid nanofluid in a rotating frame. Current Nanoscience. 2023;19(1):15-32.
16. Revathi G, Avadapu S, Raju CS, Babu MJ, Zidan AM, Alaoui MK, Shah NA, Chung JD. Dynamics of lorentz force and cross-diffusion effects on ethylene glycol based hybrid nanofluid flow amidst two parallel plates with variable electrical conductivity: A multiple linear regression analysis. Case Studies in Thermal Engineering. 2023;41:102603.
17. Ishtiaq B, Zidan AM, Nadeem S, Alaoui MK. Scrutinization of MHD stagnation point flow in hybrid nanofluid based on the extended version of Yamada-Ota and Xue models. Ain Shams Engineering Journal. 2023;14(3):101905.
18. Shah S, Hussain S, Sagheer M. MHD effects and heat transfer for the UCM fluid along with Joule heating and thermal radiation using Cattaneo-Christov heat flux model. Aip Advances. 2016;6(8):085103.
19. Khan M, Khan WA. Three-dimensional flow and heat transfer to burgers fluid using Cattaneo-Christov heat flux model. Journal of Molecular Liquids. 2016;221:651-657.
20. Xu X, Chen S. Cattaneo–Christov heat flux model for heat transfer of Marangoni boundary layer flow in a copper–water nanofluid. Heat Transfer—Asian Research. 2017;46(8):1281-1293.
21. Vasu B, Ray AK. Numerical study of Carreau nanofluid flow past vertical plate with the Cattaneo–Christov heat flux model. International Journal of Numerical Methods for Heat & Fluid Flow. 2018;29(2):702-723.
22. Ali U, Rehman KU, Malik MY. The influence of MHD and heat generation/absorption in a Newtonian flow field manifested with a Cattaneo–Christov heat flux model. Physica Scripta. 2019;94(8):085217.
23. Abu-Hamdeh NH, Alsulami RA, Rawa MJ, Alazwari MA, Goodarzi M, Safaei MR. A Significant Solar Energy Note on Powell-Eyring Nanofluid with Thermal Jump Conditions: Implementing Cattaneo-Christov Heat Flux Model. Mathematics. 2021;9(21):2669.
24. Rao DP, Thiagarajan S, Srinivas Kumar V. Significance of Dufour and Soret effects on the non-Darcy flow of Cross fluid by a tilted plate with radiation and chemical reaction: A Cattaneo–Christov heat flux model. Heat Transfer. 2022;51(2):1585-1600.

25. Purna Chandar Rao D, Thiagarajan S, Srinivasa Kumar V. Significance of quadratic thermal radiation on the bioconvective flow of Ree-Eyring fluid through an inclined plate with viscous dissipation and chemical reaction: Non-Fourier heat flux model. International Journal of Ambient Energy. 2022;43(1):6436-6448.
26. ZeinEldin RA, Ullah A, Khalifa HA, Ayaz M. Analytical Study of the Energy Loss Reduction during Three-Dimensional Engine Oil-Based Hybrid Nanofluid Flow by Using Cattaneo–Christov Model. Symmetry. 2023;15(1):166.
27. Ashraf MB, Tanveer A, Ulhaq S. Effects of Cattaneo-Christov heat flux on MHD Jeffery nano fluid flow past a stretching cylinder. Journal of Magnetism and Magnetic Materials. 2023;565:170154.
28. Makinde OD. Effects of viscous dissipation and Newtonian heating on boundary-layer flow of nanofluids over a flat plate. International Journal of Numerical Methods for Heat & Fluid Flow. 2013;23(8):1291-1303.
29. Shehzad SA, Mahanthesh B, Gireesha BJ, Shashikumar NS, Madhu M. Brinkman-Forchheimer slip flow subject to exponential space and thermal-dependent heat source in a microchannel utilizing SWCNT and MWCNT nanoliquids. Heat Transfer—Asian Research. 2019;48(5):1688-1708.
30. Alhowaity A, Bilal M, Hamam H, Alqarni MM, Mukdasai K, Ali A. Non-Fourier energy transmission in power-law hybrid nanofluid flow over a moving sheet. Scientific Reports. 2022;12(1):10406.